Maghemite Nanoparticles on Supported Diblock Copolymer Nanostructures

M. M. Abul Kashem,[†] J. Perlich,[†] L. Schulz,[†] S. V. Roth,[‡] W. Petry,[†] and P. Müller-Buschbaum*[,†]

Physik-Department LS E13, TU München, James-Franck-Str. 1, 85747 Garching, Germany, and HASYLAB at DESY, Notkestr. 85, 22603 Hamburg, Germany

Received April 2, 2007; Revised Manuscript Received May 15, 2007

ABSTRACT: Diblock copolymer nanostructures with metal oxide nanoparticles are prepared on solid supports by spin-coating. The maghemite nanoparticles (Fe_2O_3) are masked with grafted polystyrene chains to allow a tailored positioning on top of nanostructures created by the symmetric polystyrene-*block*-polyisoprene diblock copolymer. Film thickness and lamellar thickness of the diblock copolymer are smaller than the nanoparticles diameter to prevent the particles from being embedded inside the polymer superstructure. Nanostructures without nanoparticles are compared with structures with up to 30% nanoparticles content. The structural analysis is based on atomic force microscopy and grazing incidence small-angle X-ray scattering. The observed structures are explained in the framework of a retarded dewetting process preceding microphase separation. With increasing nanoparticle concentration the structural type changes from droplets into a continuous structure and covers typical lengths between 50 and 195 nm. Above a critical concentration cluster formation out of nanoparticles is present in coexistence with isolated nanoparticles and dominates structure creation.

1. Introduction

Nanocomposite materials based on a polymer matrix and inorganic nanoparticles fillers are of great importance in research because the desired physical properties can be rendered to the final product. Improving mechanical, optical, electrical, and thermal properties is still topic of ongoing research.[1−4] Target properties are largely dependent on the arrangement of nanoparticles in the host matrix used. For special application purpose an ordered arrangement of the nanoparticles is desired. An ordered arrangement of nanoparticles can be achieved by using the template offered by self-organization of block copolymers.[5−10] The idea is to incorporate nanoparticles into spherical, lamellar, or cylindrical microdomains formed by microphase separation of the block copolymer,[11−17] which can be done for example, either by removing one block and using as a mask for plating or by etching through the film and transferring the pattern to a solid substrate.[16−21] Another method is to tailor the surface of nanoparticles in a way that the block copolymer self-assembles with the nanoparticles that organize themselves selectively in one block.[22−25] Most of the work performed so far was focused on equilibrium structures as well as on films having thicknesses of several characteristic repeat units of the used diblock copolymer.

The ordered arrangement of nanoparticles is important not only in bulk but also on the surface since the surface topography influences the optical, mechanical, electrical, or thermal properties. Dewetting of thin films creates different kinds of structures on the surface depending on the molecular architecture, film thickness, interfacial energies, surface defects, fluid's viscosity, and external perturbation.[26−29] Although largely investigated, research related to dewetting is limited to polymer films and structure formation on surface based on homopolymers, polymer blends, and block copolymers without added nanoparticles.[26−37] Inorganic and organic particles can be used as fillers in the polymer matrix for suppression of dewetting. Both types of fillers give rise to different kinds of surface structures.[38−47] The inhibition of dewetting in thin filled polymer films might occur because of enrichment of filler particles at air−polymer or polymer−substrate interface. Such kind of enrichment might inhibit initiation and propagation of dewetting process by changing the interaction of polymer with the substrate followed by decreasing hydrodynamic fluid flow process during film rupture. Barnes and Karim et al. used C_{60} fullerene to suppress the dewetting process in homopolymer and reported that the inhomogeneously distributed nanofillers bind to the surface and arrest the growth of dewetting regions by pinning the contact lines of the growing holes.[38,39] Krishnan and Mackay et al. reported the similar effects using dendrimer and PS nanoparticles.[29,41] McGarrity et al. reported recently that the inhibition of dewetting due to added nanoparticles to the supported thin polymer films occurs because of migration of nanoparticles to the substrate.[48] Most of the work, so far reported, focused on stability of films on solid surface, i.e. to avoid dewetting. Lee et al.[49] reported a different approach to dewetting based on the assembly of nanoparticles by using a template offered by dewetting of charged polymer solutions. Within this investigation we are interested in nanostructures formed in the case of a symmetric diblock copolymer containing iron oxide nanoparticles. In more detail, the system consists of the symmetric diblock copolymer polystyrene-*block*-polyisoprene and maghemite nanoparticles. These iron oxide nanoparticles are coated with grafted polystyrene (PS) chains.

In the literature composite systems containing diblock copolymer films and nanoparticles were addressed by several groups.[50−57] Recently, Park et al. reported the effect of the used casting solvent on the internal morphology of the resulting diblock copolymer matrix.[54] In our investigation a comparable system in terms of polymer and nanoparticles is used. However, the work of Park et al.[54] focused on very thick, bulklike films, which are of larger thickness than the films investigated herein.

* Corresponding author. E-mail: muellerb@ph.tum.de.
[†] TU München.
[‡] HASYLAB at DESY.

10.1021/ma070782h CCC: $37.00
Published on Web 06/19/2007

The incorporation of magnetite nanoparticles into the lamellae of different thick diblock copolymer films was reported by Lauter-Pasyuk et al.[55,56] In both selected cases[54−56] the thickness of polymer film and in particular the bulk lamellar spacing were much larger than the diameter of nanoparticles embedded. In contrast, in the present work we focus on film thicknesses which are smaller than the diameter of the magnetic nanoparticles. The bulk lamellar spacing is comparable to the diameter. As a result, a completely new type of structure is obtained on top of a solid substrate. The nanoparticles cannot assemble themselves inside the lamellae domains of the diblock copolymer or inside a polymer film but arrange on top of the polymeric superstructures built up from the diblock copolymer. Thus, the structures observed exhibit freely accessible nanoparticles, which are not hidden inside a polymer matrix. Such structures are of interest for biorelated sensing applications.

The reported hybrid nanostructures are produced by spin-coating without any further processing which marks a significant difference as compared to other published work due to its simplicity. The surface structures are investigated by atomic force microscopy (AFM) using noncontact conditions to avoid tip-induced damage or structure creation on the soft polymer surface and tapping condition to get phase contrast from different materials. AFM yields topographical images and thus a typical real space information about structure heights, widths, and related statistical information such as root-mean-square (rms) roughness. Moreover, via Fourier transformation of the AFM data statistical lateral information called most prominent in-plane length is obtained. Complementary to the real-space investigation, grazing incidence small-angle X-ray scattering (GISAXS) was performed to probe these lateral structures with a higher statistical significance. In addition, GISAXS is not limited to surface structures and can probe structures formed underneath the nanoparticles and inside the polymer superstructure. The GISAXS technique is getting more and more popularity because it is a nondestructive method, which is sensitive to surface and bulk structures with a broad range of accessible structure sizes. In addition, only a very small sample volume is required.

After a short introduction to the basic experimental methods, atomic force microscopy and GISAXS, the observed structures are discussed. A summary concludes the paper.

2. Experimental Section

2.1. Sample Preparation. The used diblock copolymer polystyrene-*block*-polyisoprene, denoted P(S-*b*-I), is purchased from Polymer Standard Source (PSS, Mainz, Germany). It has a molecular weight of 23.6 kg/mol with a narrow molecular weight distribution $M_w/M_n = 1.02$ and a volume fraction of PS $f_{PS} = N_{PS}/N = 0.49$. The maghemite nanoparticles, denoted by Fe_2O_3, have a mean diameter of $D_p = 11$ nm (20% size distribution) and are covered with polystyrene (PS) chains, grafted from α-lithium polystyrenesulfonate (LPSS). The reported structures were prepared on top of precleaned silicon Si (100) surfaces. The cleaning was performed by using acidic bath (160 mL of 96% sulfuric acid, 70 mL of 30% hydrogen per oxide, and 110 mL of deionized water) at 80 °C followed by strong rinsing with deionized water.[57] The ultrathin hybrid films were prepared with spin-coating (2000 rpm for 30 s) a mixture of P(S-*b*-I) dissolved in toluene and magnetic nanoparticles dispersed in toluene on the substrates immediately after cleaning and drying. Films having different nanoparticles concentration (0, 1, 5, 10, 20, and 30 wt % in films) were prepared. During spin-coating the reported nanostructures form due to dewetting. To ensure reproducibility of the reported nonequilibrium structures, several samples were prepared under identical conditions resulting in statistically identical structures.

2.2. Atomic Force Microscopy (AFM). Local surface structures were investigated with AFM in noncontact mode operating an Autoprobe CP research AFM instrument. In noncontact mode the tip-induced damage is minimized. In special necessity we used tapping condition, too. The used gold-coated silicon cantilevers (Ultralever cantilevers) which have a resonance frequency of 60 kHz, a tip with a high aspect ratio, and an asymptotic conical shape. The radius of curvature of the tip was ∼10 nm, which is small as compared to the structures measured. The measurements were performed at room temperature in air. The AFM height and lateral calibration was performed several times with calibration standards to improve the accuracy of the height and lateral information. Because of the hardware linearization of our AFM system, this calibration works over the covered range of heights and surface area. Each scanned micrograph consists of 256 lines, scanned with 0.25 Hz up to 1.0 Hz.

The AFM measurements were carried out at different positions of the sample with different scan sizes (typically 0.5, 1, 2, 4, and 8 μm). Only the topographical and no phase shift information was obtained in noncontact mode. Tapping mode gave us phase contrast among hard solid surface, hard nanoparticles, and soft polymer (no phase contrast image is reported in this article). From the raw data the background due to the scanner tube movement was fully subtracted.

The root-mean-square (rms) roughness of the sample surface representing the deviation of individual heights from a mean surface was calculated by using the Image Processing (IP 1.3) software. The rms roughness statistically describes structures perpendicular to the surface.[58]

To obtain statistical lateral information about the probed structures, the power spectral density (PSD) function was calculated.[59] The first step in this calculation is the two-dimensional Fourier transformation of the height data probed with the AFM. It gives a two-dimensional (2d) intensity distribution in reciprocal space. The desired PSD function results after a radial averaging of such a 2d intensity distribution. Figure 1 shows an example of an AFM topography image; its Fourier transformed intensity distribution and PSD function. In such a way, the AFM data of all scan sizes produced a set of PSD functions that were merged into a (so-called) master curve,[60] as shown in Figure 1c. This master curve represents the statistics of length scales of lateral structures in reciprocal space on the overall probed surface area. The master curves are comparable to the GISAXS cuts described later.

2.3. Grazing Incidence Small-Angle X-ray Scattering (GISAXS) Measurements. To resolve the structures present on top and inside the polymer nanostructure, the surface-sensitive X-ray scattering technique grazing incident small-angle X-ray scattering (GISAXS) was used. The basic setup of the GISAXS scattering geometry is shown schematically in Figure 2. GISAXS measurements were carried out at the beamline BW4 of the DORIS III storage ring at HASYLAB (DESY, Hamburg). The selected wavelength was $\lambda = 0.138$ nm. The beam divergence in and out of the plane of reflection was set by two entrance cross-slits. The beam was moderately focused to the size of ($H \times B$) 30×60 μm^2 by using an assembly of refractive beryllium lenses.[61] The sample was placed horizontally on a goniometer. A beam stop was used to block the direct beam in front of the detector. Besides, a second, pointlike movable beam stop was also used to block the specular peak on the detector. The incident angle was set to $\alpha_i = 0.72°$, which is well above the critical angles of the polymers (0.138°) and nanoparticles (0.28°). As a result, specular and Yoneda peak are well separated on the detector, and both the sample surface and the film are probed. Because of the shallow incident angle, the footprint of the X-ray beam on the sample surface was 2.4 mm long. The scattered intensities were recorded by a 2d detector (MARCCD; 2048 × 2048 pixel) positioned at $D_{SD} = 1.97$ m behind the sample. A characteristic GISAXS pattern is shown in Figure 2. Because of its simple shape, structural information is obtained from vertical and horizontal cuts of the 2d intensity distribution.[62] The vertical cut at $q_y = 0$, called detector cut, contains the information on the structure perpendicular

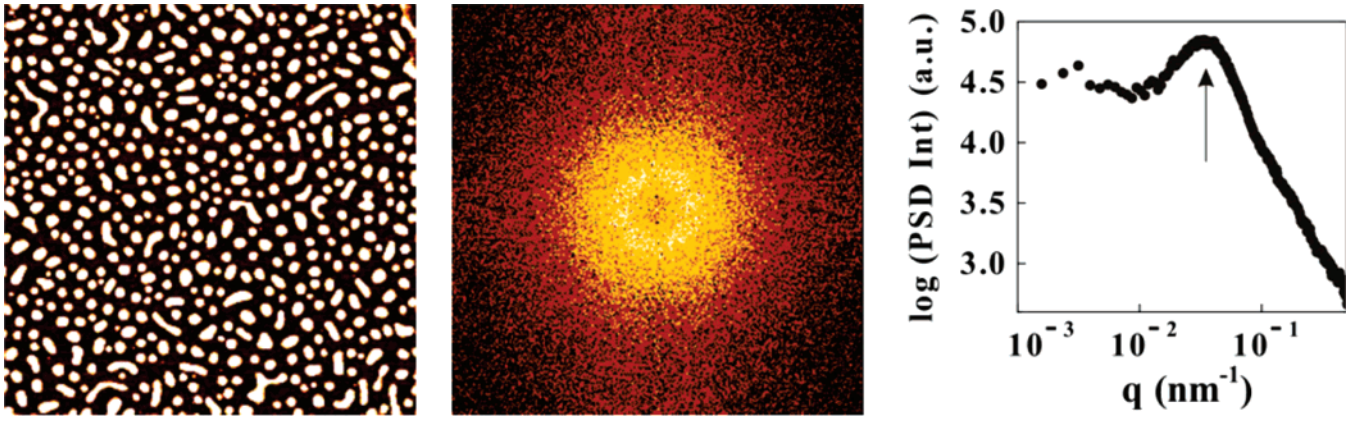

Figure 1. Example of master curve generation from AFM data. **(a)** Topography data of scan size 4 μm × 4 μm measured in noncontact mode presenting the droplike structures from dewetting of diblock copolymer film. Brightness represents the structure's height. **(b)** Calculated two-dimensional Fourier transformed image, showing the ring of intensity (sign of an isotropic structure) in Fourier space. **(c)** Master curve formed by combining power spectral density (PSD) functions that resulted from radial averaging of intensity distribution in Fourier space of different scan ranges. The position of the peak shown by the arrow relates to the most prominent in-plane length.

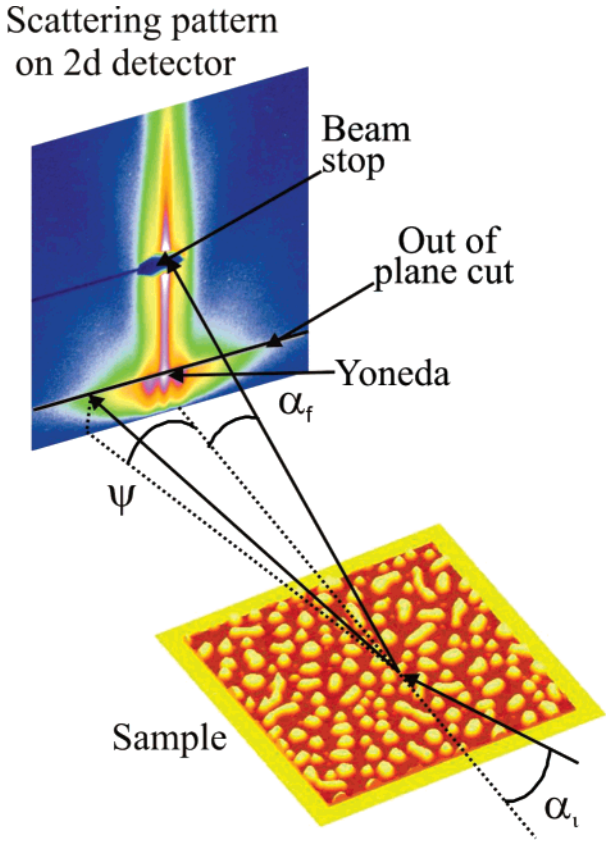

Figure 2. Schematic picture of the experimental setup in GISAXS geometry. The sample surface is placed horizontally. The incident angle is denoted α_i, the exit angle α_f, and the out-of-plane angle ψ. The two-dimensional detector resembles along the horizontal axis the q_y dependence and along the vertical axis the q_z dependence (neglecting the small q_x dependence). The scattering intensity distribution on the detector (low intensity as dark and high intensity as bright) is presented on a logarithmic scale. The detected scattering pattern shows the diffuse scattering with the split Yoneda peak and specular peak (shielded by a beam stop that protects the detector from a very high intensity of the reflected beam), which are common features of a nanostructured surface.

to the surface. Horizontal cuts at constant q_z allow extracting the information (geometry, size distribution, and spatial correlation) of lateral structures.[63] The intensity of the q_y cuts was integrated over a small slice Δq_z in the vertical direction to obtain an improved statistics. In the literature these horizontal cuts are also named as GISAXS cuts and out-of-plane cuts.

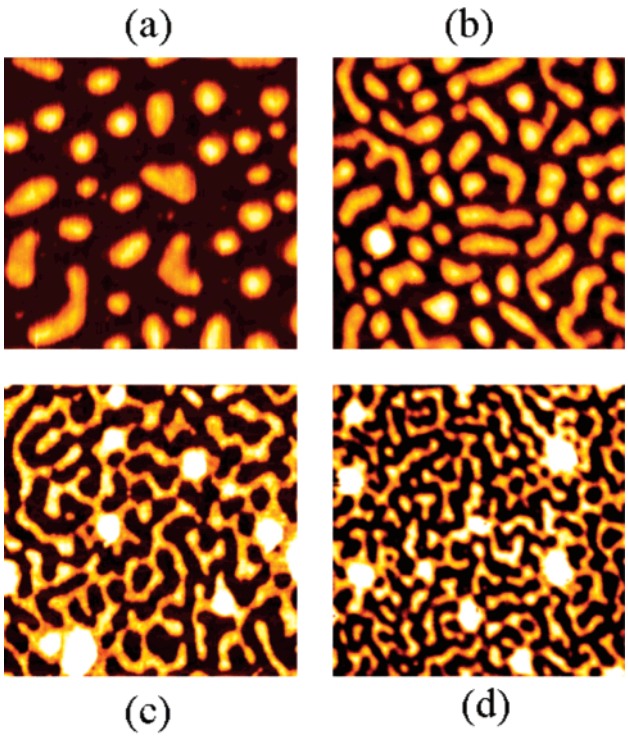

Figure 3. AFM micrographs show a scan size of 1 μm × 1 μm to emphasize local structures (a, 0%; b, 1%; c, 20%; d, 30% by weight of nanoparticles). The structure heights increase with the increase in brightness of structures in the images.

3. Results and Discussion

All reported structures were formed directly during the spin-coating process. On a macroscopic scale as probed with optical techniques no preferential structures are observable. X-ray reflectivity proves the absence of homogeneous layers which are parallel to the substrate surface. As a consequence, high-resolution techniques which are sensitive to lateral structures are applied.

3.1. Surface Structures. Surface structures of the created nanostructures are investigated by AFM. The surface topography of the produced structures as a function of nanoparticle concentration is shown on a small scale in Figure 3. The sample without added nanoparticles, the pure P(S-*b*-I) nanostructure (see Figure 3a), consists of individual droplets, which are typical for dewetted ultrathin polymer films.[30,31] Since no additional

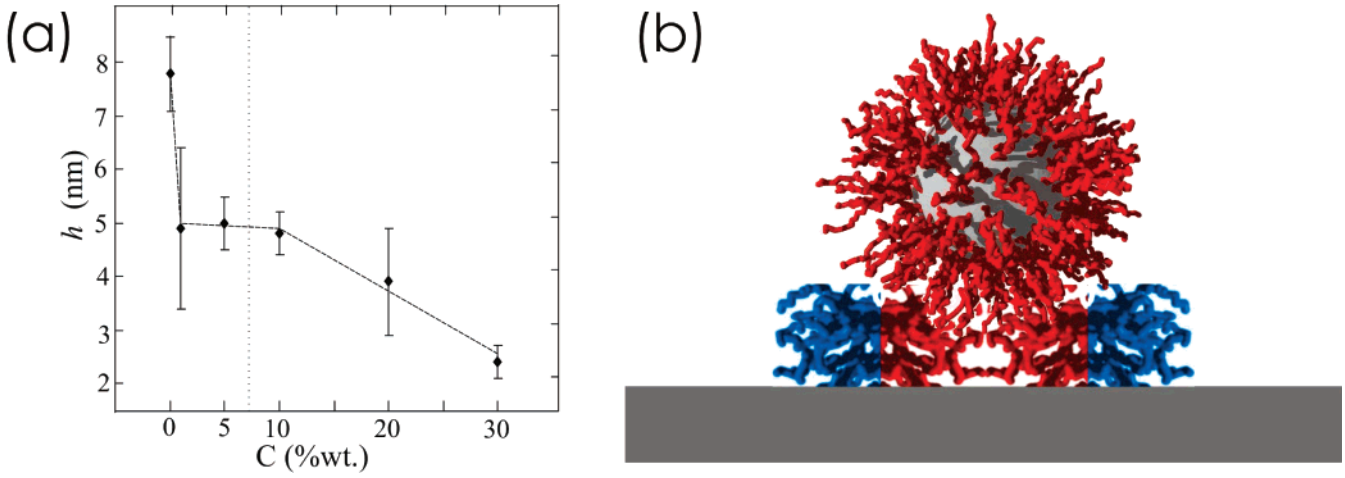

Figure 4. (a) Height h of the polymer structures without nanoparticles, as measured by AFM, displayed as a function of the nanoparticles concentration C. The dashed line is a guide to the eye to visualize the decrease in heights. **(b)** Schematic side view picturing the PS masked nanoparticle sitting on top of the diblock copolymer nanostructure on a solid support.

sample treatment was applied, these structures are created through spin-coating the polymer solution on the hydrophobic silicon wafer surface. The film formation through spin-coating is a three-step process which is described elsewhere.[60] This structure formation does not take place in the first and second steps where fluid's inertia, its surface tension, shear thinning effects, and balance between viscous flow and centrifugal force dominate. It results in the third step which is characterized by the presence of a highly viscous homogeneous toluene−polymer solution. Upon solvent evaporation this very thin film gets unstable and decays into isolated droplets as it was observed in the case of homopolymers and block copolymers.[64,65] No homogeneous layer of the diblock copolymer is formed below a critical concentration of polymer in the spin-coated solution.[65] Polymer droplets are formed on the substrate because of dewetting and the insufficient material to form a complete layer. Height and width of the resulting structures are $h \sim 7.8$ nm and $w \sim 118$ nm, respectively. The symmetric diblock copolymer used in the present investigation has a bulk lamellar morphology with a bulk lamellar period of $L = 13.2$ nm[66,67] (and thus a lamellar thickness $L/2 < D_p$). The height of the nanostructures, as probed with AFM, is not commensurate with the bulk lamellar period L or distances of $L/2$. Consequently, it is unlikely that a lamellae parallel to the substrate is present inside the islands. However, AFM could not provide information about the presence of perpendicularly oriented lamellae either.

The surface topography of the samples changes with the addition of nanoparticles. The resulting nanostructure appears more densely packed. The nanoparticles are located on top of the diblock copolymer superstructure. No nanoparticles are observed on the bare silicon substrate. In general, the localization of maghemite nanoparticles within the different diblocks or at the interfaces between the diblocks is driven by a competition between entropy and enthalpy. On the one hand, any localization of the nanoparticles reduces their entropy and is therefore disfavored. On the other hand, putting nanoparticles coated with one type of polymer (in this investigation PS) in contact with a different polymer (such as polyisoprene) costs enthalpy (or energy) relative to putting it in contact with the same polymer (e.g., PS). This is the primary driving force behind the localization of the nanoparticles at different places within the diblock copolymer phases.[50,51] Because of the chosen system with particle diameters larger than the lamellar spacing and the height of the nanostructures, an incorporation of the nanoparticles is energetically unfavorable. On the other hand, because of very fast drying process during spin-casting and the entanglement between PS chains grafted on the maghemite nanoparticles and the diblock copolymer chains particles could not migrate to the substrate. As a result, single nanoparticles and clusters of nanoparticles are present on top of the polymeric superstructure. In the case of single particles, enthalpic interaction might lead the nanoparticle to stay on the PS phase. This phenomenon is shown in Figure 4b as a sketch, which does not show microphase separation but the probable position of a single nanoparticle on dewetted diblock copolymer superstructure.

At very low nanoparticle concentration (1% and 5%) the dropletlike structures are replaced by wormlike structures. Comparable to the observation in polymer films of larger film thickness,[39] the presence of nanoparticles retards the dewetting and thus inhibits the droplet formation, which is typical for the final stage of dewetting. As a result of a retarded dewetting, the height of the polymer structures decreases from 8 to 5 nm and the surface area covered with polymer material increases (see Figure 3). The retardation process continues with increasing amount of nanoparticles. Figure 4a displays the decrease in the height of the polymer nanostructures as a function of the nanoparticle concentration. The height information is extracted from AFM images with 1 μm scan size. In addition, the width of these structures decreases significantly from 105 ± 9 nm (0% np) to 55 ± 9 nm (20% np) and 49 ± 9 nm (30% np). However, the statistics of this information is limited since they are based only on a small surface area.

Above a critical concentration of nanoparticles a second process of structure formation starts. Nanoparticle clusters consisting of several nanoparticles (in Figure 3 visible as the big bright objects) dominate structure formation. This kind of cluster formation might be due to the entanglement among the PS chains masking the iron oxide core. These clusters are present in addition to single nanoparticles and positioned on the polymer nanostructures as well. Again, no clusters are found on the dewetted bare parts of the substrate. We attribute this special location of clusters as well to the presence of PS chains on the surface of iron oxide nanoparticles which comprise into the clusters. Because of this masking, the nanoparticles are preferentially attached to the PS block of the diblock copolymer and thus stay in the polymer phase. Above a critical concentration, at very high nanoparticle contents (20% and 30%), the number of clusters strongly increases.

In Figure 5 a larger scan range is shown for an improved visualization of the developed clusters. Because of the second

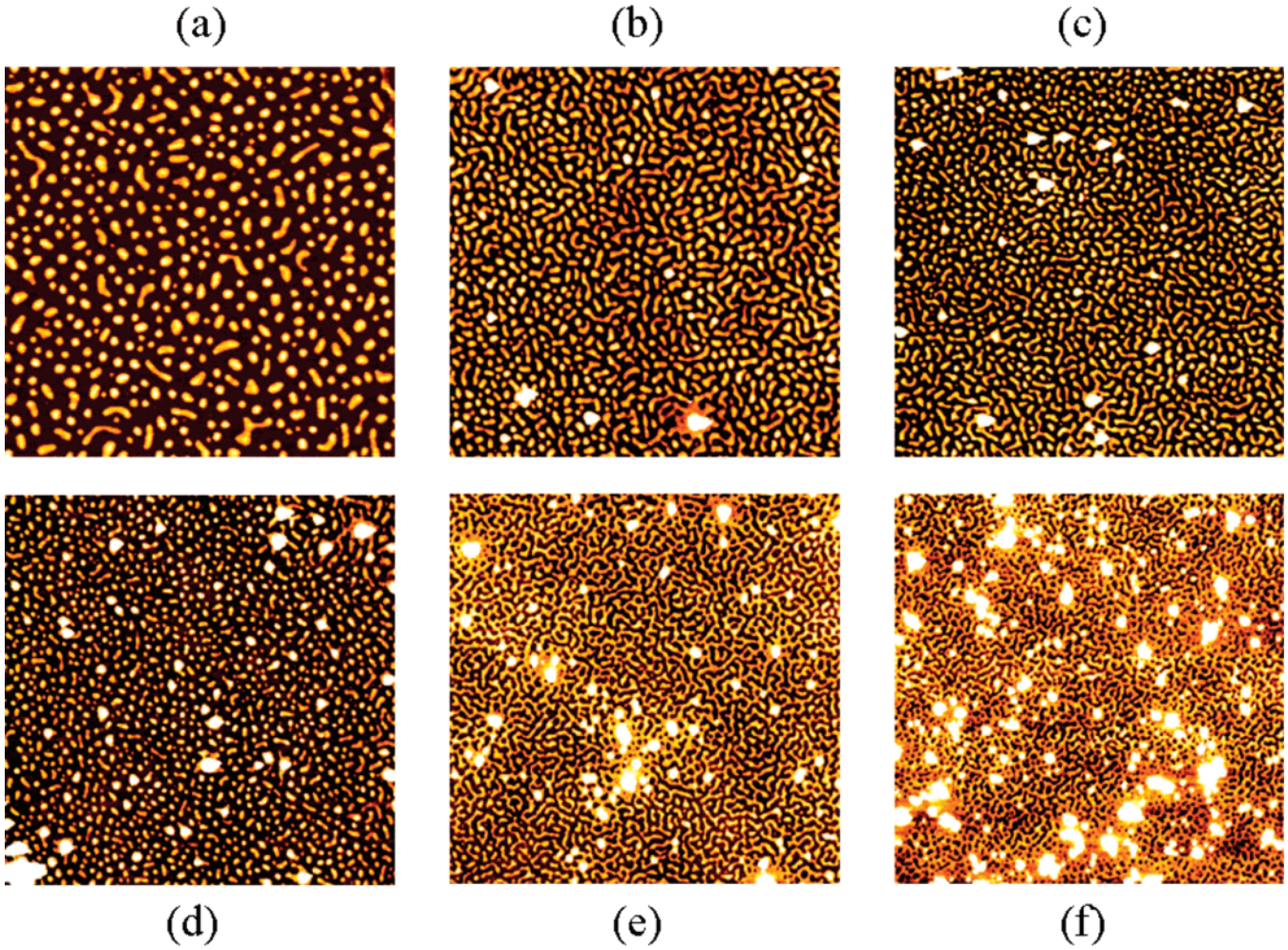

Figure 5. AFM micrographs showing the surface topography of the nanostructures which result from the addition of different amounts (a, 0%; b, 1%; c, 5%; d, 10%; e, 20%; f, 30% by weight) of nanoparticles and cluster formation at high nanoparticle concentrations. The scan size is 4 μm $\times$ 4 μm. Structure height increases with the brightness of the structure in the images.

process, the domination of clusters at higher nanoparticles concentration, the regular continuous polymer structures do not convert into a continuous polymer film with increasing amount of nanoparticles. However, the distance between two adjacent polymer structures decreases with increasing amount of nanoparticles.

To obtain statistical information about the lateral length scales of the structures on the sample surface, AFM data are Fourier transformed and a so-called master curve is constructed out of data measured with different scan ranges.[56] This master curve construction is described in the Experimental Section in more detail (see Figure 1). Figure 6 shows a plot of the master curves.

The master curve of the sample without added nanoparticles (bottom curve in Figure 6) exhibits a peak at $q^* = 3.22 \times 10^{-2}$ nm^{-1}. This peak corresponds to the most prominent in plane length of the polymer structures on the substrate surface. The corresponding lateral length is $d = 2\pi/q^* = 195$ nm and is given by the distance between two neighboring diblock copolymer droplets. With increasing concentration of nanoparticles (1 and 5%) the related peak becomes less pronounced and shifts toward larger q values. This shift indicates a decrease in the lateral distance. At higher nanoparticle concentrations the peak in the master curve is hardly visible. The presence of the clusters strongly dominates the surface structure. Although the clusters are attached to the polymer nanostructure, they remain randomly positioned on top of the polymer part and exhibit no lateral order. As a consequence, the master curve from the AFM data

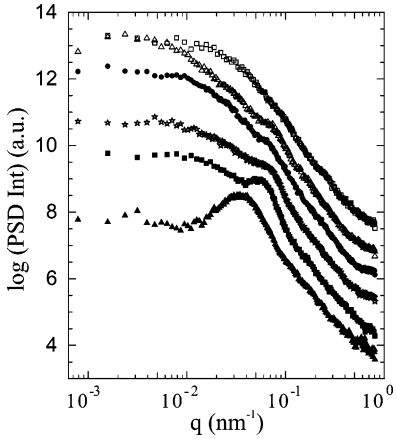

Figure 6. Double-logarithmic plot of PSD master curves for samples containing varying amount of nanoparticles (from bottom to top the nanoparticle concentration increases: 0, 1, 5, 10, 20, and 30% by weight). For a better understanding the master curves are shifted along PSD intensity axis (y-axis).

results in less well-pronounced intensity maxima as compared to simple polymer nanostructures.[31] The determined values of peak positions are 130, 88, 105, 119, and 65 nm for samples containing 1%, 5%, 10%, 20%, and 30% nanoparticles, respectively. As discussed above, the population density of the polymer structures (droplets, wormlike, and regular continuous) increases

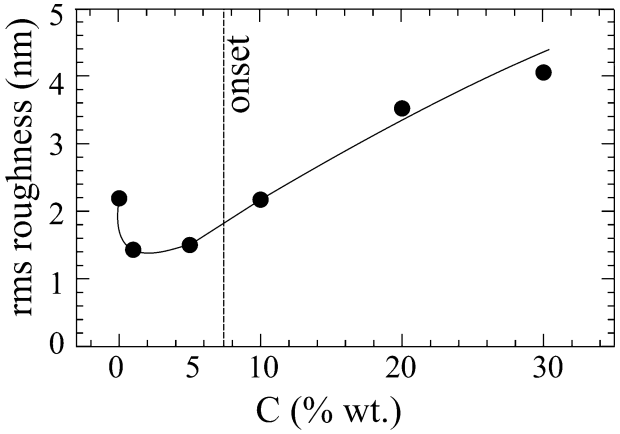

Figure 7. Rms roughness of the nanostructures including the nanoparticles as a function of the nanoparticle concentration *C* determined with AFM. The solid line is a guide to the eye.

with increasing amount of nanoparticles; i.e., the distance between neighboring lateral structures decreases.

It is noteworthy that there exists a second peak at small values $q \sim 5.5 \times 10^{-3}$ nm^{-1} present in samples which include nanoparticles. This peak is attributed to the distances between nanoparticles which are not located in clusters. Because the peak is not well-defined and the statistics are poor due to the limited surface area scanned with AFM, no related distances are determined.

A statistical information perpendicular to the sample surface is given by the rms roughness. The values of rms roughness are plotted against nanoparticles concentration in Figure 7. The initial roughness of the silicon substrate was subtracted from the values measured with the AFM image processing software. Therefore, the plotted values represent the roughness due to the nanostructures (polymer with nanoparticles) only. The values of the rms roughness decreases by the addition of nanoparticles, and it remains almost constant at low nanoparticle concentrations. At higher concentration it increases continuously. The initial decrease is explained by the decrease of structure heights due to the retardation of dewetting. At small nanoparticle concentrations the ongoing decrease is compensated by the formation of nanoparticle clusters. At higher concentration the increasing amount of clusters increases the rms roughness, which underlines that for these sample clusters dominate the sample surface.

3.2. Buried Structures. Data and images provided by AFM picture the surface topography. Although the nanostructures are very limited in height, AFM data cannot give information about the internal structures inside these nanostructures and under the clusters. To address these buried structures, the samples were investigated with X-ray scattering. The common small-angle X-ray scattering in transmission geometry (SAXS) requires a bulk sample because the beam passes through the sample volume. With decreasing scattering volume such as in ultrathin films as the system described within this article, the transmission geometry is no longer applicable.[63] Therefore, we used grazing incident small-angle X-ray scattering (GISAXS), a technique in which the transmission geometry is replaced by reflection geometry. The resulting surface sensitivity enables the investigation of surfaces and thin films with thickness down to the sub-monomolecular range.[68−70] Consequently, GISAXS is sensitive to the nanostructures which are investigated herein.

Figure 8 displays the corresponding 2d intensities measured at the samples containing different amounts of nanoparticles. In general, the 2d intensities show marked features in the

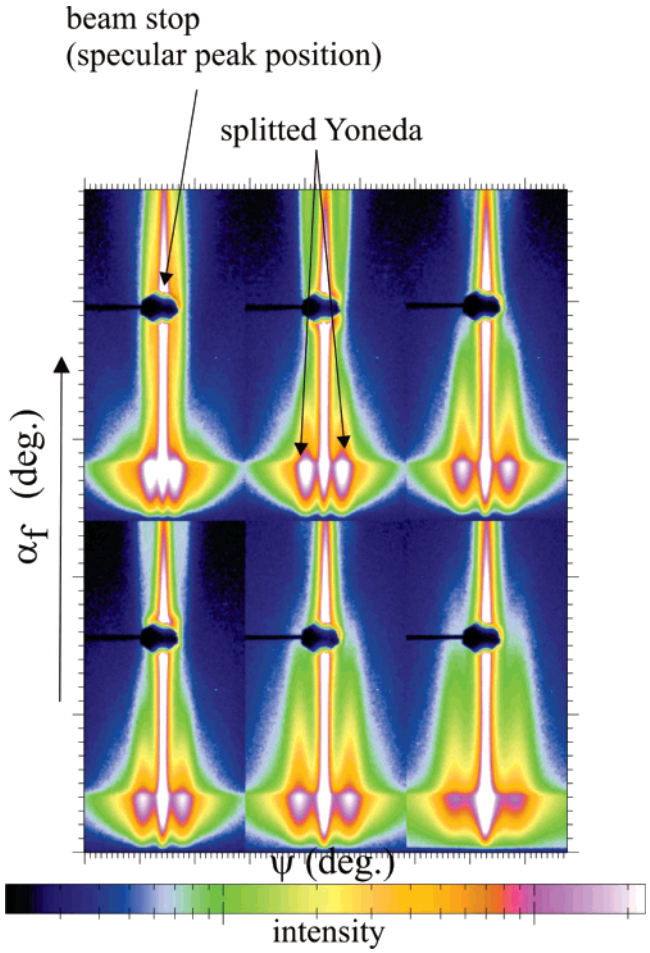

Figure 8. Composite image showing 2d GISAXS scattering patterns measured at samples with different nanoparticle concentrations. The top three images have 0, 1, and 5% (from left to right) and the bottom three have 10, 20, and 30% (from left to right) nanoparticle concentration. In each 2d image the out-of-plane angle ψ is plotted along the *x*-axis and the exit angle α_f along the *y*-axis. The intensity is shown on a logarithmic scale. The color coding was chosen to emphasize the features in the diffuse scattering (black/blue = low and white = high intensity—see scale bar). The Yoneda and beam stop shielding the specular peak are marked by arrows.

intensity. Because of the chosen incident angle, the specular peak (shielded by beam stop) is well separated from the Yoneda peak. There is no modulation in the intensity arising from the Yoneda peak toward the specular peak. The absence of such intensity modulation results from the missing correlation in structures between the substrate surface and nanostructures.[63] Thus, the nanostructures are individually shaped and positioned on top of the substrate as to be expected in the case of dewetting. The common feature in all 2d intensities is the splitting of the Yoneda peak in the out-of plane direction ψ. This splitting is due to well-defined lateral structures. Only a very limited polydispersity in structural distances allows observing such an intensity distribution.[63] The presence of intensity in the center of the Yoneda peak is due to the presence of additional large lateral structures which are not resolved in the scattering experiment. Correspondingly, the intensity maxima due to the splitting of the Yoneda peak occur as side maxima to this central maximum in the intensity in the corresponding line cuts. With change in the nanoparticle concentration the position of the side maxima shifts along q_y.

The change in the allover shape of the Yoneda side maxima as a function of the exit angle α_f reflects the changes in the height of the nanostructures. However, a simple horizontal cut

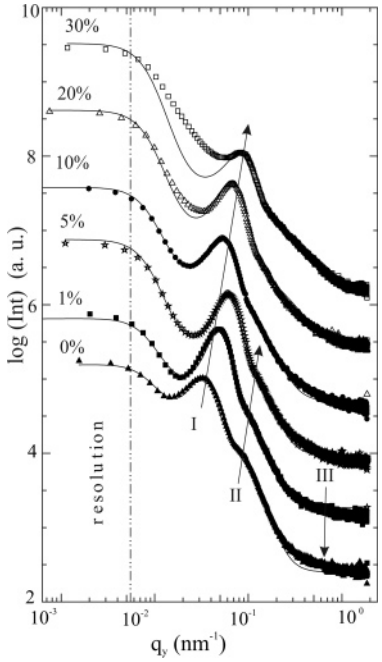

Figure 9. Double-logarithmic plot of out-of-plane cuts (symbols) of the 2d intensity as a function of the q_y component of the scattering vector. The solid lines are the fit lines for determining the most prominent in-plane length scale. The curves are shifted along the intensity axis for clarity. From the bottom to the top the nanoparticle concentration increases as indicated. The dashed line indicates the resolution limit of the experiment. The two dominant structures are marked with I and II and position of the expected microphase separation structure with III. The arrows display the shift with changing nanoparticle concentration.

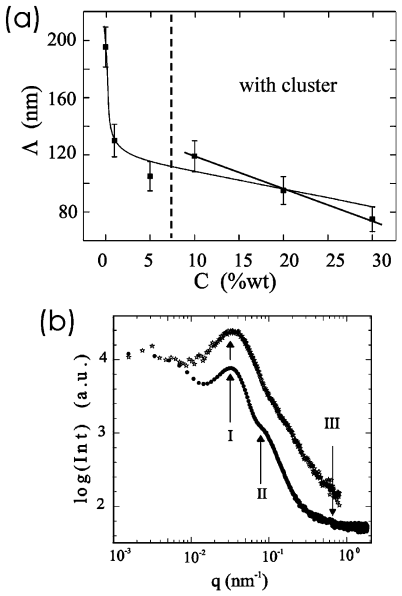

Figure 10. (a) The most prominent in-plane lengths Λ of the structure related to peak I in Figure 9 plotted as a function of the nanoparticle concentration *C*. The solid lines are guides to the eye. The dashed line indicates the critical concentration for cluster formation. **(b)** Example of a comparison between the out-of-plane cut (filled circles) and the PSD master curve (stars) in the case of the sample containing no nanoparticles. The curves are shifted along *y*-axis for clarity. The arrows show the most prominent in-plane lengths corresponding to structures as explained in the text.

from an individual 2d intensity is sufficient to extract the relevant structural information about the lateral structures. The full treatment of the 2d intensities is not necessary due to the simple scattering patterns.

The selected horizontal cuts are made at an exit angle equal to the critical angle of the component of one block (in this case PS) present in the diblock copolymer P(S-*b*-I) to become more sensitive to this component. Figure 9 shows a plot containing all these cuts as a function of the nanoparticle concentration. The intensities are plotted as a function of the component of the scattering vector q_y, which is oriented parallel to the sample surface and perpendicular to the X-ray beam. The strong peak in these cuts corresponds to the highly ordered surface structures present. The position of the peak is determined by a model fit to the data taking into account the form and structure factors as well as the resolution function. The resolution function is defined by the largest detectable in-plane length scales of the sample Λ and is determined by the sample-to-detector distance and the used X-ray optics. Form and structure factors are assumed to have a Lorentzian size distribution. The lateral length introduced by a microphase separation structure was not included into the fit because its contribution is small. The expected position is marked III in Figure 9.

In the data of the sample containing no nanoparticles one strong peak at $q = 3.22 \times 10^{-2}$ nm^{-1} and one weak peak at $q = 6.35 \times 10^{-2}$ nm^{-1} are observed. The strong peak is common in all samples irrespective of nanoparticle concentration, but its position and width are changing with nanoparticle concentration. The weak peak is visible only in films containing no or low amounts of nanoparticles. It vanishes at higher nanoparticle concentration. In Figure 9 the strong peak is marked with I and the weak one with II. No strong peak is found at the position expected in the case of formation of a perpendicularly oriented lamellae from the P(S-*b*-I).

The positions of both peaks, denoted I and II, are determined from the model fits. The corresponding values of the structure factor of peak I are plotted as a function of the nanoparticle concentration in Figure 10a. We identify these lateral lengths with the distances between two neighboring structures (droplets or others) due to the missing correlation between the nanoparticles and the clusters. Thus, GISAXS probes the polymer nanostructures irrespective of the present nanoparticles.

Because all structures are created during the spin-coating and are frozen in by the solvent evaporation, the formed structures belong to different stages of the dewetting of the ultrathin highly concentrated solution layer. Within the error limit a clear decrease of these distances of adjacent structures with increasing nanoparticles concentration is observed. The decrease is very big upon the addition of a very small amount of nanoparticles (change 0−1%) reflecting the retardation in the dewetting. With further addition of nanoparticles the decay is less strong and for a limited concentration regime appears linear with concentration. Thus, the amount of nanoparticles controls the kinetics of dewetting by changing the viscosity of dewetting nanocomposite. In general, the higher the amount of nanoparticles, the slower is the dewetting kinetics. In more detail, including cluster formation and the presence of a critical concentration (as indicated by the dashed line in Figure 10a), the two-step character of the retardation of the dewetting becomes visible. At low concentrations of nanoparticles the retardation proceeds with the adding of nanoparticles. At the onset of cluster formation, nanoparticles go into clusters and decrease the effective concentration of nanoparticles acting in retardation. Thus, the structures observed at 10% nanoparticle concentration seem not to be that strongly retarded as expected without cluster formation. As a consequence, the lateral structures are larger (or in other words less retarded in dewetting upon the solid substrate) than at 5% nanoparticle concentration.

The weak structure factor peak II corresponds to a second smaller lateral length which is assigned with the diameter of the polymer structures on the substrate. We can identify this peak in Figure 9 only in films having 0, 1, and 5% nanoparticles. Its position shifts with increasing nanoparticle concentration toward smaller q_y values. The determined diameters are 99, 92.5, and 80 nm in film containing 0, 1, and 5% nanoparticles, respectively. These values are quite similar to values as obtained by AFM image analysis within standard deviation limit.

The thickness of the films are below the lamellar period, i.e. $d < L$, and the widths of the structures are either nL or $nL + {}^1/_2$. It is already known that the lamellar structure perpendicular to the substrate can be observed when the thickness of symmetric diblock copolymer film is smaller than the bulk lamellar period. Therefore, we expected that the formed structures contain perpendicular lamellar microdomains, which could be formed by shearing during spin-coating. But only a very weak contribution to the GISAXS signal is found of the position corresponding to 13.2 nm (marked as III in Figure 10b) in the case of no added nanoparticles. This small contribution is visible due to the difference between data and fit in the bottom curve in Figure 9. With added nanoparticles the fit can explain the measured data which demonstrates that in a statistical meaning no lamellar spacing due to a microphase separation structure is present. Besides, the phase contrast of AFM image does not show any perpendicular lamellar microdomains.

In samples at higher nanoparticle concentrations of 10, 20, and 30%, we find no relationship between the lamellar period and the width of the observed structures. Thus, these cluster sizes and their distributions were not resolved. As a consequence, we see that the fitting curves do not match with the data at very low q in Figure 9. We assume that this is because of the presence of a structure factor peak related to big clusters of nanoparticles which is not resolved in the scattering experiment and thus only influence the intensity at very low q.

For a final comparison, the results obtained with AFM following the master curve construction and an out-of-plane cut from the GISAXS measurement are shown together in Figure 10b. We restrict the comparison to the sample without nanoparticles because as outlined above the addition of nanoparticles changes the meaning of both data sets. As obvious from Figure 10b, peak positions (denoted I) in both curves are the same and both peaks have a similar broadness in both curves. This means that the lateral length scales of distances between neighboring polymer nanostructures are similar to that in the overall film structures seen with GISAXS. Thus, the AFM images and data are representative of the overall film structures in terms of distances of adjacent polymer nanostructures. The peak at $q = 6.35 \times 10^{-2}$ nm^{-1} (denoted II) present in the GISAXS data is not present in AFM data because it represents the shape of the polymer nanostructures, and AFM delivers only a very limited statistics as compared to the scattering experiment. The structural length related to microphase separation (denoted III) is only probed with GISAXS because the master curves were constructed from topography data of AFM in noncontact mode. As a result, we see only the external height changes of the surface. The internal phase changes cannot be detected by topography data in noncontact condition. But the GISAXS measurement gives an average statistics of the structures inside the film as well.

4. Conclusion

A new type of nanostructures comprising of maghemite nanoparticles masked by PS chains sitting on top of polymer superstructures is investigated. Because of the special selected spatial sizes of nanoparticles, lamellar thickness of diblock copolymer in bulk, and film thickness, this new type of nanocomposite is formed. The particles are too big in size to allow for incorporation inside a diblock copolymer lamellae of the polymer matrix. The film thickness is too small to allow establishing homogeneous films consisting of lamellae which are oriented parallel to the substrate. Moreover, the film thickness is that small, that dewetting is observed on the sample surface. The presence of PS chains on iron oxide core causes entanglement with polymer chains and thus prevents migration to substrate and results an arrangement of nanoparticles on top of polymer superstructures. With increasing amount of nanoparticles the dewetting is retarded, however, not suppressed. As a consequence, nanostructures formed by the diblock copolymer are observed for all investigated nanoparticles concentrations (up to 30%). The reason for clusters formation in the films might be the entanglement of polymer chains grafted on nanoparticles. As a consequence, with addition of more and more nanoparticles (after onset) the number of clusters increases but no continuous film is produced, suppressing dewetting.

The major advantage is originating from the simplicity of the preparation, which basically relies on cleaned Si surfaces and the spin-coating of the polymer−nanoparticle mixture. No special and dedicate additional treatments are necessary. Nevertheless, the resulting structures are highly reproducible and well controlled in terms of the installed lateral order of the polymer structures. At low concentration nanoparticles distribute themselves with regular distances on the polymeric superstructures. Because of the grafted PS chains, the nanoparticles are only observed on top of the polymer nanostructures (see Figure 4b). The preparation techniques allows for reaching very high nanoparticle concentrations, which in thicker films (and thus higher concentrated solutions necessary in the spin-coating) will become impossible due to the rapid increase in viscosity. Drawback is the onset of cluster formation at high nanoparticles concentrations. Ways to overcome this clustering might be an improved perfection of the PS masking and a reduction in the polydispersity of the nanoparticle diameters. However, despite the presence of clusters, the reported structures can be of interest for biorelated sensing applications, which require freely accessible nanoparticles. To allow for molecular recognition and biosensors, an additional preparation step will become necessary to remove the PS chains from the nanoparticles. With respect to sensing, the absolute position of the nanoparticles is of less interest, whereas it is of high importance that the nanoparticles are not located inside a polymer matrix but attached to it.

Acknowledgment. We thank the Bavarian State Ministry of Sciences, Research and Arts for funding this research work through International Graduate School "Materials Science of Complex Interfaces" (CompInt).

References and Notes

(1) Bockstaller, M.; Kolb, R.; Thomas, E. L. *Adv. Mater.* **2001**, *13*, 1783.
(2) Shenton, W.; Pum, D.; Sleytr, U. B.; Mann, S. *Nature (London)* **1997**, *389*, 585.
(3) Alexandre, M.; Dubois, P. *Mater. Sci. Eng.* **2000**, *28*, 1.
(4) Akcora, P.; Zhang, X.; Varughese, B.; Briber, M. R.; Kofinas, P. *Polymer* **2005**, *46*, 5194.
(5) Kim, S. H.; Misner, M. J.; Xu, T.; Kimura, M.; Russell, T. P. *Adv. Mater.* **2004**, *16*, 226.
(6) Russell, T. P. *Curr. Opin. Colloid Interface Sci.* **1996**, *1*, 107.
(7) Haryono, A.; Binder, H. W. *Small* **2006**, *2*, 600.
(8) Shenhar, R.; Norsten, T. B.; Rotello, V. M. *Adv. Mater.* **2005**, *17*, 657.

(9) Green, P. F.; Christensen, T. M.; Russell, T. P. *J. Chem. Phys.* **1990**, *92*, 1478.
(10) Seul, M.; Andelman, D. *Science* **1995**, *265*, 476.
(11) Spatz, J. P.; Mossmer, S.; Hartmann, C.; Moller, M.; Herzog, T.; Krieger, M.; Boyen, H. G.; Ziemann, P.; Kabius, B. *Langmuir* **2000**, *16*, 407.
(12) Lopes, W. A.; Jaeger, H. M. *Nature (London)* **2001**, *414*, 735.
(13) Horiuchi, S.; Fujita, T.; Hayakawa, T.; Nakao, Y. *Langmuir* **2003**, *19*, 2963.
(14) Templin, M.; Franck, A.; DuChesne, A.; Leist, H.; Zhang, Y. M.; Ulrich, R.; Schadler, V.; Wiesner, U. *Science* **1997**, *278*, 1795.
(15) Li, M.; Schnablegger, H.; Mann, S. *Nature (London)* **1999**, *402*, 393.
(16) Thurn-Albrecht, T.; Schotter, J.; Kastle, C. A.; Emley, N.; Shibauchi, T.; Krusin-Elbaum, L.; Guarini, K.; Black, C. T.; Tuominen, M. T.; Russell, T. P. *Science* **2000**, *290*, 2126.
(17) Akcora, P.; Briber, R. M.; Kofinas, P. *Polymer* **2006**, *47*, 2018.
(18) Bates, F. S.; Fredrickson, G. H. *Annu. Rev. Phys. Chem.* **1990**, *41*, 525.
(19) Hashimoto, T.; Txutsumi, K.; Funaki, Y. *Langmuir* **1997**, *13*, 6869.
(20) Thurn-Albrecht, T.; Steiner, R.; DeRouchey, J.; Stafford, C. M.; Huang, E.; Bal, M.; Tuominen, M.; Hawker, C. J.; Russell, T. P. *Adv. Mater.* **2000**, *12*, 787.
(21) Park, M.; Harrison, C.; Chaikin, P. M.; Register, R. A.; Adamson, D. H. *Science* **1997**, *276*, 1401.
(22) Lauter-Pasyuk, V.; Lauter, H. J.; Ausserre, D.; Gallot, Y.; Cabuil, V.; Kornilov, E. I.; Hamdoun, B. *Physica B* **1997**, *241*, 1092.
(23) Hamdoun, B.; Ausserre, D.; Joly, S.; Gallot, Y.; Cabuil, V.; Clinard, C. *J. Phys. II* **1996**, *6*, 493.
(24) Lefebure, S.; Cabuil, V.; Ausserre, D.; Paris, F.; Gallot, Y.; Lauter-Pasyuk, V. *Prog. Colloid Polym. Sci.* **1998**, *110*, 94.
(25) Lin, Y.; Böker, A.; He, J.; Sill, K.; Xiang, H.; Abetz, C.; Li, X.; Wang, J.; Emrick, T.; Lung, S.; Wang, Q.; Balazs, A.; Russell, T. P. *Nature (London)* **2005**, *434*, 55.
(26) Barnes, K. A.; Douglas, J. F.; Liu, D. W.; Bauer, B.; Amis, E. J.; Karim, A. *Polym. Int.* **2000**, *49*, 463.
(27) Sehgal, A.; Ferreiro, V.; Douglas, J. F.; Amis, E. J.; Karim, A. *Langmuir* **2002**, *18*, 7041.
(28) Gu, X.; Raghavan, D.; Douglas, J. F.; Karim, A. *J. Polym. Sci., Part B: Polym. Phys.* **2002**, *40*, 2825.
(29) Krishnan, R. S.; Mackay, M. E.; Hawker, C. J.; Horn, B. V. *Langmuir* **2005**, *21*, 5770.
(30) Green, P. F. *J. Polym. Sci., Part B: Polym. Phys.* **2003**, *41*, 2219.
(31) Müller-Buschbaum, P.; Gutmann, J. S.; Stamm, M. *J. Macromol. Sci., Phys*. **1999**, *B38*, 577.
(32) Sharma, A.; Khanna, R. *Phys. Rev. Lett.* **1998**, *81*, 3463.
(33) Xie, R.; Karim, A.; Douglas, J. F.; Han, C. C.; Weiss, R. A. *Phys. Rev. Lett.* **1998**, *81*, 1251.
(34) Segalman, R.; Green, P. F. *Macromolecules* **1999**, *32*, 801.
(35) Ashley, K. M.; Raghavan, D.; Douglas, J. F.; Karim, A. *Langmuir* **2005**, *21*, 9518.
(36) Ashley, K. M.; Meredith, J. C.; Amis, E.; Raghavan, D.; Karim, A. *Polymer* **2003**, *44*, 769.
(37) Meredith, J. C.; Smith, A. P.; Karim, A.; Amis, E. J. *Macromolecules* **2000**, *33*, 9747.
(38) Barnes, K. A.; Douglas, J. F.; Liu, D. W.; Karim, A. *Adv. Colloid Interface Sci.* **2001**, *94*, 83.
(39) Barnes, K. A.; Karim, A.; Douglas, J. F.; Nakatani, A. I.; Gruell, H.; Amis, E. J. *Macromolecules* **2000**, *33*, 4177.
(40) Krishnan, R. S.; Mackay, M. E.; Hawker, C. J. *Poly. Mater. Sci. Eng.* **2004**, 91.
(41) Mackay, M. E.; Hong, Y.; Jeong, M.; Hong, S.; Russell, T. P.; Hawker, C. J.; Vestberg, R.; Douglas, J. F. *Langmuir* **2002**, *18*, 1877.
(42) Briber, R.; Feng, H.; Lee, V.; Kim, H. C.; Miller, R. *APS March Meeting Bull.* **2004**, R1.035.
(43) Holmes, M. A.; Mackay, M. E.; Giunta, R. K. *Polym. Mater. Sci. Eng.* **2004**, 91.
(44) Krishnan, R. S.; Mackay, M. E.; Duxbury, P. M.; Pastor, A.; Hawker, C. J.; Van Horn, B.; Asokan, S.; Wong, M. S. *Nano Lett.* **2007**, *7*, 484.
(45) Xavier, J. H.; Sharma, S.; Seo, Y. S.; Isseroff, R.; Koga, T.; White, H.; Ulman, A.; Shin, K.; Satija, S. K.; Sokolov, J.; Rafailovich, M. H. *Macromolecules* **2006**, *39*, 2972.
(46) Sharma, S.; Rafailovich, M. H.; Peiffer, D.; Sokolov, J. *Nano Lett.* **2001**, *1*, 511.
(47) Feng, Y.; Karim, A.; Weiss, R. A.; Douglas, J. F.; Han, C. C. *Macromolecules* **1998**, *31*, 484.
(48) McGarrity, E. S.; Frischknecht, A.; Mackay, M. E. *APS March Meeting Bull.*, 2007.
(49) Lee, L. T.; Leite, C. A. P.; Galembeck, F. *Langmuir* **2004**, *20*, 4430.
(50) Kim, B. J.; Chiu, J. J.; Yi, G.-R.; Pine, D. J.; Kramer, E. J. *Adv. Mater.* **2005**, *17*, 2618.
(51) Chiu, J. J.; Kim, B. J.; Kramer, E. J.; Pine, D. J. *J. Am. Chem. Soc.* **2005**, *127*, 5036.
(52) Spatz, J.; Mossmer, S.; Möller, M.; Kocher, M.; Neher, D.; Wegner, G. *Adv. Mater.* **1998**, *10*, 473.
(53) Boontongkong, Y.; Cohen, R. E. *Macromolecules* **2002**, *35*, 3647.
(54) Park, M. J.; Char, K.; Park, J.; Hyeon, T. *Langmuir* **2006**, *22*, 4,1376.
(55) Lauter-Pasyuk, V.; Lauter, H. J.; Gordeev, G. P.; Müller-Buschbaum, P.; Toperverg, B. P.; Jernenkov, M.; Petry, W. *Langmuir* **2003**, *19*, 7783.
(56) Lauter-Pasyuk, V.; Lauter, H. J.; Gordeev, G. P.; Müller-Buschbaum, P.; Toperverg, B. P.; Petry, W.; Jernenkov, M.; Petrenko, A.; Aksenov, V. *Physica B* **2004**, *350*, e939.
(57) Müller-Buschbaum, P. *Eur. Phys. J.* **2003**, E 12, 443.
(58) Russ, J. C. *Fractal Surface*; Plenum: New York, 1971.
(59) Bendat, J. S.; Piersol, A. G. *Random Data: Analysis and Measurement Procedures*; Wiley-Interscience: New York, 1971.
(60) Gutmann, J. S.; Müller-Buschbaum, P.; Stamm, M. *Faraday Discuss.* **1999**, *112*, 285.
(61) Roth, S. V.; Döhrmann, R.; Dommach, M;. Kuhlmann, M.; Kröger, I.; Gehrke, R.; Walter, H.; Schroer, C.; Lengeler, B.; Müller-Buschbaum, P. *Rev. Sci. Instrum.* **2006**, *77*, 085106.
(62) Salditt, T.; Metzer, T. H.; Peisel, J.; Reinker, B.; Moske, M.; Samwer, K. *Europhys. Lett.* **1995**, *32*, 331.
(63) Müller-Buschbaum, P. *Anal. Bioanal. Chem.* **2003**, *376*, 3.
(64) Müller-Buschbaum, P.; Bauer, E.; Wunnicke, O.; Stamm, M. *J. Phys.: Condens. Matter* **2005**, *17*, S363.
(65) Stange, T. G.; Mathew, R.; Evans, D. F.; Hendrickson, W. A. *Langmuir* **1992**, *8*, 920.
(66) DeRouchey, J.; Thurn-Albrecht, T.; Russell, T. P. *Macromolecules* **2004**, *37*, 2538.
(67) Hashimoto, T.; Shibayama, M.; Kawai, H. *Macromolecules* **1980**, *13* 1237.
(68) Müller-Buschbaum, P.; Vanhoorne, P.; Scheumann, V.; Stamm, M. *Europhys. Lett.* **1997**, *40*, 655.
(69) Müller-Buschbaum, P.; Stamm, M. *Physica B* **1998**, *248*, 229.
(70) Müller-Buschbaum, P.; Casagrande, M.; Gutmann, J. S.; Kuhlmann, T.; Stamm, M.; Cunis, S.; Krosigk, G. von; Lode, U.; Gehrke, R. *Europhys. Lett.* **1998**, *42*, 517.

MA070782H